PAPER

Highly Reliable Silica-$LiNbO_3$ Hybrid Modulator Using Heterogeneous Material Integration Technology

Atsushi ARATAKE[†*a)], *Senior Member*, Ken TSUZUKI[††], Motohaya ISHII[†††**], Takashi SAIDA[††], Takashi GOH[††], Yoshiyuki DOI[††], Hiroshi YAMAZAKI[†], Takao FUKUMITSU[†], Takashi YAMADA[††], *and* Shinji MINO[†††**], *Members*

SUMMARY Silica-$LiNbO_3$ (LN) hybrid modulators have a hybrid configuration of versatile passive silica-based planar lightwave circuits (PLCs) and simple LN phase modulators arrays. By combining the advantages the two components, these hybrid modulators offer large-scale, highly-functionality modulators with low losses for advanced modulation formats. However, the reliability evaluation necessary to implement them in real transmissions has not been reported yet. In terms of reliability characteristics, there are issues originating from the difference in thermal expansion coefficients between silica PLC and LN. To resolve these issues, we propose design guidelines for hybrid modulators to mitigate the degradation induced by the thermal expansion difference. We fabricated several tens of silica-LN dual polarization quadrature phase shift keying (DP-QPSK) modulators based on the design guidelines and evaluated their reliability. The experiment results show that the modules have no degradation after a reliability test based on GR-468, which confirms the validity of the design guidelines for highly reliable silica-LN hybrid modulators. We can apply the guidelines for hybrid modules that realize heterogeneous device integration using materials with different coefficients of thermal expansion.

key words: *modulator, PLC, lithium niobate, reliability, hybrid module*

1. Introduction

Recently, 400-Gb/s technologies have been commercialized in wavelength-division-multiplexing (WDM) transmission systems with multilevel format using digital coherent technologies or pulse modulation method such as pulse amplitude modulation (PAM), and research and development are focusing on miniaturization and function enhancement to achieve front density integration of optical communication equipment. Hybrid integration, which combines the physical performance limits of individual materials, is an attractive technology for achieving miniaturization and high performance of optical modules, and has been extensively studied. We have already proposed several types of modulators with spectrally efficient transmission characteristics by combining both the fast response of the LN and the excellent transparency of the silica-based PLC [1]–[10]. They are suitable for advanced modulation formats, such as multi-carrier or flexible formats over 100 Gb/s, and can be constructed with the same basic assembly structure.

However, as a problem of hybrid integration, there is a concern about an influence on optical characteristics due to a difference in physical constants, especially a difference in thermal expansion coefficients. In the silica-LN modulator, there is an order of magnitude difference in the thermal expansion coefficient between the silica-PLC and the LN waveguide substrate. Furthermore, the reliability of the silica-LN modulator has not been thoroughly investigated. This may induce optical coupling losses and thermal stress in the lateral and axial directions, respectively, with changes in the environmental temperature. Thus, for real network implementations, it is necessary to devise design guidelines for silica-LN modules to mitigate the degradations and verify the reliability of modules fabricated based on the design guidelines.

In a previous work, we estimated the waveguide positional misalignment and thermal stress of a silica-LN modulator module by simulation and a partial experiment. On the basis of these results, we proposed design guidelines with which the characteristic degradation in silica-LN modulator modules can be avoided with environmental changes in reliability tests [11]. In this paper, we describe the results of additional reliability tests performed on silica-LN hybrid-integrated modulator modules in the laboratory and discuss their reliability in detail. We fabricated some tens of modules and evaluated their reliability to confirm the validity of the design guidelines. The results show that we achieved reliability that complies with the Telcordia-0468 (GR-468) standard. In Sect. 2, we describe the basic structure and concept and explain the reliability issues. In Sect. 3, then we propose and discuss the design guidelines for reliability. Finally, we show the results of reliability tests of the silica-LN modulators to confirm our design guidelines in Sect. 4.

2. Basic Structure

2.1 Concept of Silica-LN Modulators

Figure 1 shows the basic structure of a silica-LN hybrid integrated modulator, which consists of a LN chip with an array of phase modulators and two silica-based PLCs. The

Manuscript received September 2, 2019.
Manuscript revised December 5, 2019.
Manuscript publicized February 13, 2020.

[†]The authors are with NTT Device Technology Laboratories, NTT Corporation, Atsugi, Kanagawa, 243–0198 Japan.
[††]The authors are with NTT Device Innovation Center, NTT Corporation, Atsugi-shi, 243–0198 Japan.
[†††]The authors are with the NTT Electronics Corporation, Yokohama-shi, 221–0031 Japan.
[*]Presently, with NTT Access Network Service Systems Laboratories, NTT Corporation.
[**]This work was performed at the NTT Photonics Laboratories, NTT Corporation.
a) E-mail: atsushi.aratake.hf@hco.ntt.co.jp

DOI: 10.1587/transele.2019ECP5044

Copyright © 2020 The Institute of Electronics, Information and Communication Engineers

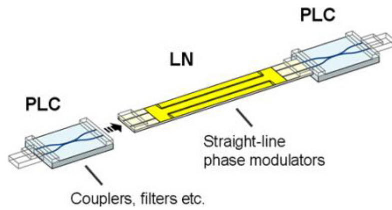

Fig. 1 Basic Structure of silica-LN hybrid modulator.

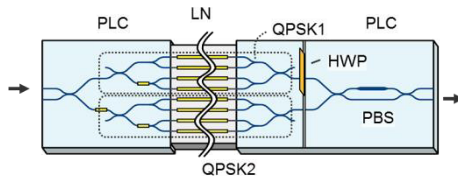

Fig. 2 Configuration of the fabricated DP-QPSK modulator.

LN waveguide has an excellent electro-optic effect and has already been commercialized as a high-speed modulator. In this LN chip, the active components are arrayed simple straight-line high-speed phase modulators. On the other hand, the PLCs contain all the passive components, such as the optical splitter, polarization beam combiner (PBC), and WDM filters for orthogonal frequency-division multiplexing (OFDM). The combination of these two mature technologies as shown in Fig. 1 yields a flexible and large-scale integrated modulator for advanced formats. Various kinds of modulators with this basic structure can be fabricated by changing the number of phase modulators in the LN chip and the circuit design of the PLCs.

The DP-QPSK modulator in Fig. 2 is a typical example with the same structure. Here we describe the structure of the silica-LN hybrid modulator in more detail. In more advanced modulators, the configuration is the same as in this example, although the number of arrays of LN phase shifter waveguides and the size of each chip are different. It consists of an LN chip with an array of eight straight phase modulators and two silica PLCs with couplers, a polarization rotator with a half-wavelength plate (HWP), and a waveguide PBC. The LN and silica PLCs are butt-coupled with UV curable adhesive by using the conventional active alignment technique. This is a mature technique originating from the assembly of silica PLCs and optical fiber arrays. Optical fiber blocks are also butt-coupled to the PLC with UV curable adhesive.

Figure 3 (a) and (b) shows schematics of the structure in an overview and cross section of the portion of a silica-LN hybrid modulator along an optical axis in the module package, respectively. In the module, the silica-PLC-LN chip is bonded to a stainless-steel (SUS: Steel use stainless) package as shown in Fig. 3 (a). Figure 4 is a photograph of the DP-QPSK module. The module is 131-mm long, including fiber boots at both ends, 13.5-mm wide, and 7-mm high. This is one of the smallest sizes, including both fiber booths, ever reported for such a module.

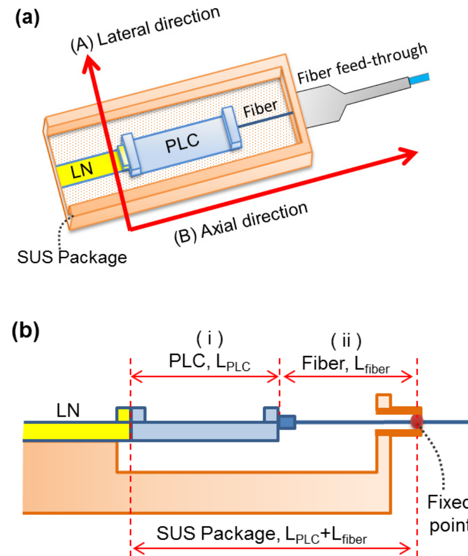

Fig. 3 (a) Schematic structure of a portion of a silica-LN hybrid modulator in the module package. (b) Schematic cross-section of the silica-LN modulator along an optical axis.

Fig. 4 Photograph of silica-LN DP-QPSK modulator which size is 118 mm long, 13.5 mm wide, and 7 mm height.

Table 1 Thermal expansion coefficient of constituent materials.

Element	Coefficient (ppm/K)
Optical Fiber	0.75
Silica-PLC(Si substrate)	2.5
LN	15.4
SUS Package	17.3

2.2 Reliability Issues

The silica-LN modulator module consists of a silica PLC on a Si substrate, a LN chip, optical fiber, and a SUS package as shown in Fig. 3. However, there are differences in the thermal expansion coefficients among these materials (Table 1). Here we use a SUS package which has a thermal expansion coefficient close to that of LN to avoid the thermal stress between the LN chip and package. Thus, the thermal expansion coefficients of the optical fiber and silica-PLC, whose substrate is silicon, are much smaller than those of the LN chip and SUS package.

Accordingly, there are two reliability issues for the silica-LN modulators caused by the thermal expansion difference. First, in the lateral direction of the optical axis between the silica-PLC and LN, the LN chip expands much

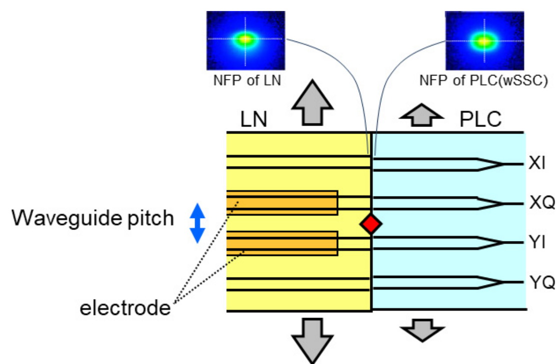

Fig. 5 Position shift between LN and PLC by increasing temperature.

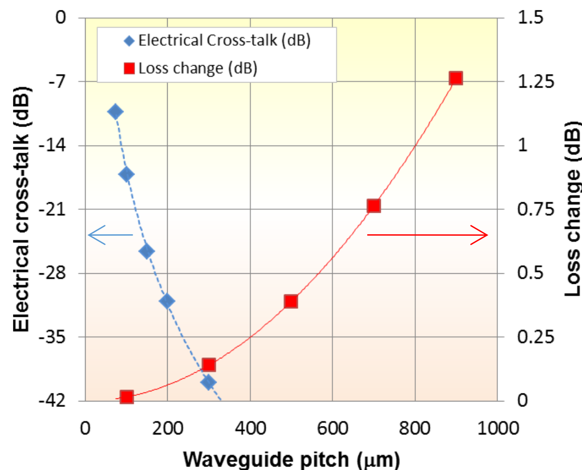

Fig. 6 Relationship between the optical loss change/electrical crosstalk and the waveguide pitch.

more than the PLCs when the temperature increases as shown in Fig. 5. As a consequence, the positions of waveguides on the PLC and LN chip shift relative to each other because the adhesive between the PLC and the LN chip is not hard enough to keep them in place. This alignment positional mismatch caused by ambient temperature change gives rise to excess coupling loss between a PLC and the LN chip.

Secondly, in the axial direction, the issue is thermal stress resulting from large thermal expansion of the LN and SUS package compared to the silica-PLC and optical fiber as temperature increases. The LN chip is directly bonded to a SUS package, which has a thermal expansion coefficient close to that of LN. The PLCs and optical fibers are butt-coupled consecutively using adhesive. And the fibers are soldered to the fiber feed-through at each end of the package to form hermetic seals, as shown in Fig. 3 (b). Thus, as the temperature increases, the SUS package expands much more than the PLC chips and the fibers. Accordingly, the PLC chips and the optical fibers receive tensile stress from the package at a high temperature.

3. Design

To solve these problems, we estimated the characteristic degradation and thermal stress by thermal simulations and high-frequency electromagnetic simulations and also performed partial experiments for the verification. On the basis of the results, we devised design guidelines to ensure the reliability of the silica-LN integrated modules. In this section, we describe the design guidelines regarding the lateral and axial directions.

3.1 Lateral Direction

In the lateral direction, as mentioned above, the issue is that the waveguides of silica and LN shift relative to each other at the connection boundary between a silica PLC chip and LN chip, as shown in Fig. 5. Near-field patterns of PLC and LN waveguides are shown above the figure of the hybrid chip. The PLC waveguide is equipped with a spot-size converter at the edge of the chip. The coupling loss between the PLC waveguide and the LN waveguide is about 0.4 dB. This waveguide positional mismatch gives rise to small excess coupling losses as temperature increases.

As shown in Fig. 6, if we decrease the pitch of the waveguides, induced losses are decreased as temperature increases. On the other hand, the small pitch increases the electrical crosstalk between the radio frequency (RF) electrodes. Thus, we calculated these characteristics and analyzed this trade-off quantitatively. The optical coupling losses between the silica PLC and LN for the outermost waveguides induced by the temperature change (−5 to 75°C) were approximately calculated by the simple Gauss beam overlap model. The solid line in Fig. 6 shows that an optical loss change is decreased to less than 0.3 dB as the waveguide pitches are decreased below 400 μm. On the other hand, electrical crosstalk was calculated analytically by using the approximate model of conventional parallel coplanar waveguides (CPWs). The dotted line in Fig. 6 shows the results of these calculations performed by using these rough models. A CPW corresponds to a pair of optical waveguides, and waveguide pitch is defined as the distance between the CPWs. The electrical crosstalk is reduced to less than −28 dB at a frequency of 20 GHz as the waveguide pitches are increased to more than 200 μm. Therefore, we selected the waveguide pitch of 300 μm with low optical loss change of less than 0.3 dB and adjacent electrical crosstalk of less than −25 dB. Figure 7 shows frequency responses of the electrical crosstalk on the adjacent CPWs in an actual module prototype when the waveguide pitch is about 300 μm. Although the crosstalk from adjacent YI to YQ is slightly larger, the electrical crosstalk is suppressed below −25 dB.

3.2 Axial Direction

For the axial direction, the thermal expansion coefficient of the SUS package is much larger than that of the PLC and optical fiber as mentioned above. Thus, the PLC and optical

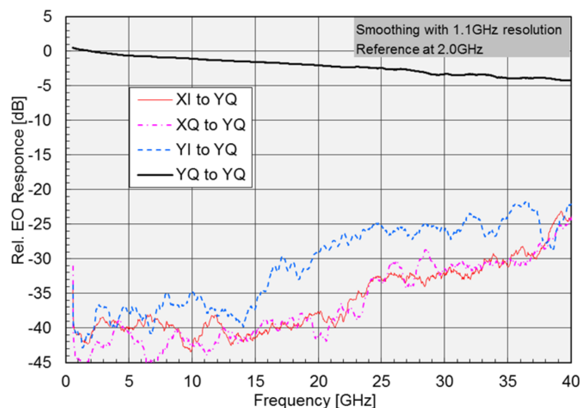

Fig. 7 Electrical crosstalk for the CPWs on LN substrate.

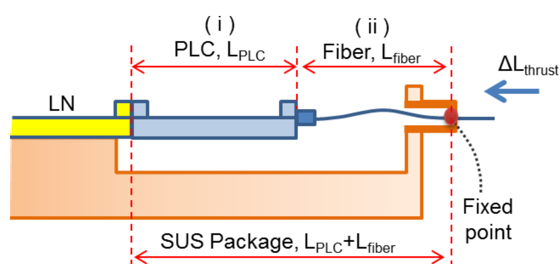

Fig. 8 Schematic cross-section of the modulator with fiber bending.

fiber are stretched by the package in Fig. 3 (b) as temperature increases; this stretch may induce a break in the fiber in the worst case. Therefore, we pushed the fiber in the thrust length $\Delta L_{\mathrm{thrust}}$ inside the package before soldering it to produce a small bend to mitigate the effects of thermal stretching stress as the temperature increases, as shown in Fig. 8. However, if we push the fiber into the package too far, the fiber will bend too much; this bend induces a bending break in the fiber. Thus, we have to estimate the suitable structural parameter range of fiber thrust length $\Delta L_{\mathrm{thrust}}$ as a parameter of optical fiber length L_{fiber} as shown in Fig. 3 (b) by simulation and experiment to avoid fracture due to bending.

First, we estimated the condition where the optical fiber doesn't receive tensile stress from the package. We calculate the expansion length difference between the optical fiber plus the PLC and the SUS package as the temperature increases. In region (i) in Fig. 8, the expansion length difference ΔL_{PLC} between the PLC and SUS package with the temperature increase of ΔT is shown as $\Delta L_{\mathrm{PLC}} = L_{\mathrm{PLC}}(\beta - \alpha)\Delta T$. Here the thermal expansion coefficient (α, β) is for the Si substrate and the SUS package. Similarly, the expansion length difference $\Delta L_{\mathrm{fiber}}$ between the optical fiber and SUS package in region (ii) is shown as $\Delta L_{\mathrm{fiber}} = L_{\mathrm{fiber}}(\beta - \gamma)\Delta T$. The parameter γ is the thermal expansion coefficient of the optical fiber. Therefore, the total length difference ΔL_{tot} between the PLC and fiber and the package is shown as $\Delta L_{\mathrm{tot}} = \{(\beta - \alpha) L_{\mathrm{PLC}} + (\beta - \gamma) L_{\mathrm{fiber}}\} \Delta T$.

When $\Delta L_{\mathrm{thrust}} (1 + \gamma\Delta T)$ is lower than ΔL_{tot}, the fiber receives strong tensile force from the package and may break. Therefore, $\Delta L_{\mathrm{thrust}}$ has to be designed under the following condition if the term of $\Delta L_{\mathrm{thrust}}\, \gamma\Delta T$ is negligibly small.

$$\Delta L_{\mathrm{thrust}} > \{(\beta - \alpha)L_{\mathrm{PLC}} + (\beta - \gamma)L_{\mathrm{fiber}}\}\Delta T \quad (1)$$

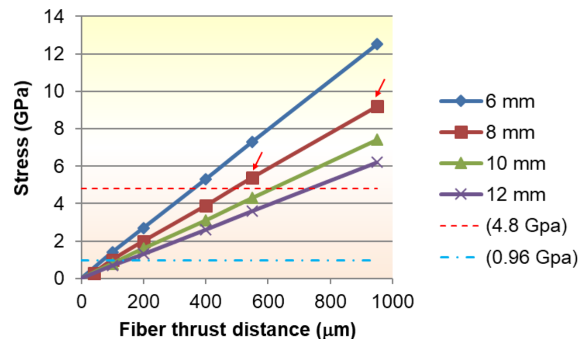

Fig. 9 Relationship between fiber stress and fiber thrust distance.

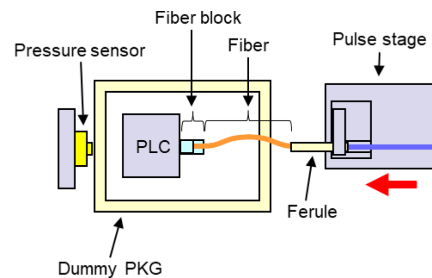

Fig. 10 Experimental setup for the fiber stress test.

Next, we estimated the condition where the fiber bending rupture with fiber thrust can be avoided. We first calculated the stress of fiber when we thrust the fiber with $\Delta L_{\mathrm{thrust}}$ by simulation with the finite element method. Figure 9 shows the dependence of stress in the optical fiber on $\Delta L_{\mathrm{thrust}}$ as a parameter of fiber length L. In this simulation, we assumed the PLC length is 20 mm, which corresponds to the typical size of a PLC comprising high-functionality and large optical circuits. Here, the typical tensile fracture strength of a conventional optical fiber is reported to be 6 kgf [12], [13]. We estimated the tensile fracture stress to be 4.8 GPa (indicated as a dotted line in Fig. 9), considering the optical fiber diameter is 125 μm [14]. In the estimation of mechanical strength in optical fiber, it is said that we have to set up a safety coefficient of at least 5, considering a risk margin [15]. Thus, we decided that the target stress value should be less than 0.96 GPa, as shown in Fig. 9 by a dashed-dotted line.

We also estimated the relationship between the rupture stress and the thrust distance ΔL by experiment because the fiber in the module is metal-coated and the stress and rupture strength may be different from the ideal bare fiber we simulated above. Figure 10 shows a schematic of the experimental setup. The compact fiber block was bonded to the PLC with UV curable adhesive, and this PLC with optical fiber was bonded on the dummy package with adhesive. The optical fiber of length of 8 mm with metal ferule was thrust with a common precise pulse stage. The fiber broke at the thrust distances of 570 and 950 μm. These values

correspond to the stress of 5.4 and 9.2 GPa, respectively. The results are shown in Fig. 9 as red arrows. These typical values show that the thrust fracture values in this experiment correspond to our calculated fracture stress.

Furthermore, we measured the dependence of the buckling force of the optical fiber on the fiber thrust distance ΔL using the experimental setup in Fig. 10. Here the stage under the package can be moved freely, and the optical fiber is not fixed to the package and can move freely. Therefore the stress of the optical fiber was directly measured with a pressure sensor just at the opposite side of the package to the fiber. Figure 11 shows buckling stress dependence of fiber thrust distance ΔL. The fiber stress is about 60 gf when ΔL is 100 μm. The typical buckling stress of bare fiber is reported to be 56 gf when the fiber length L is 8 mm [16]. This value is almost equal to our experimental values. These results show that our fibers have almost the same buckling force as our values calculated from the mechanical properties of optical fiber.

We plot the relationship between thrust length $\Delta L_{\mathrm{thrust}}$ and fiber feed length L_{fiber} in Fig. 12. From the fiber stretching viewpoint, we show the result calculated from (1) as a dashed-dotted line in Fig. 12. Thus, the optical fiber in the region where $\Delta L_{\mathrm{thrust}}$ is below the dashed-dotted line indicates the risk of stretch fracture damage to the fiber at that point. We also plot the results of the rupture experiment as two triangle marks in Fig. 12. On the other hand, from

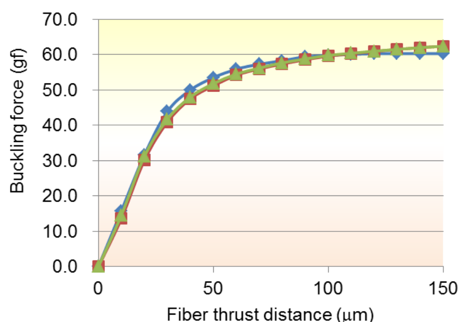

Fig. 11 Relationship between buckling force and fiber thrust distance $\Delta L_{\mathrm{thrust}}$.

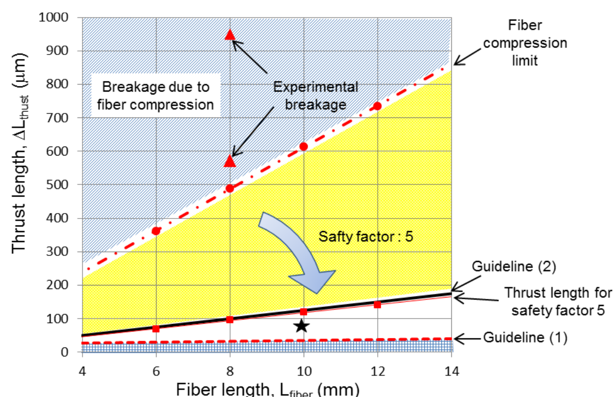

Fig. 12 Relationship between fiber length L_{fiber} and fiber thrust distance $\Delta L_{\mathrm{thrust}}$.

the fiber compression viewpoint with thrust, the red dashed-dotted line is thrust rupture stress of 4.8 GPa, and the solid red line is that of 0.96 GPa which is one-fifth, considering the safety factor of 5 as described above. Here, the safety region is approximately described as

$$\Delta L_{\mathrm{thrust}} < 0.0125\ L_{\mathrm{fiber}}. \tag{2}$$

We illustrated the region that satisfies (2) in Fig. 12, where $\Delta L_{\mathrm{thrust}}$ is below the solid black line.

From the above considerations, we can set up the guidelines of (1) and (2) along the optical axis for fiber feed length L_{fiber} and thrust distance $\Delta L_{\mathrm{thrust}}$ to avoid the breakage due to tensile force and fiber compression by thermal expansion. In these guidelines, we use the relation $\beta \gg \gamma$ from a practical viewpoint. As a result, the optical fiber in the region where $\Delta L_{\mathrm{thrust}}$ is above the solid line indicates the risk of compression damage to the fiber at that point. This region is between the straight line and the dashed-dotted line in Fig. 12.

When we design a practicable module for a silica-LN modulator, we have to shorten L_{fiber} to make the module compact. However, the shorter L_{fiber} is, the narrower the tolerance to changing $\Delta L_{\mathrm{thrust}}$ becomes for the assembly. Considering this tradeoff, in practical modules, we set L_{fiber} and $\Delta L_{\mathrm{thrust}}$ at 10 mm and about 75 μm, respectively. These parameters are illustrated as a star plot in Fig. 12. We fabricated some tens of DP-QPSK modules using this design guideline, and we evaluated the reliability characteristics to verify this guideline. We have to judge the validity of this design guideline for reliability from the module reliability results. As described in the next section, we measured the basic characteristics the fabricated DP-QPSK modules and evaluated the reliability following the Telcordia-0468 tests.

4. Reliability Results

4.1 Initial Properties

We used the guidelines to fabricate several tens of modules for 100G DP-QPSK modulators. Typical characteristics of the modulators are listed in Table 2. Our module is fully compliant and compatible with the Optical Internetworking Forum (OIF) 100G standard. It has a low insertion loss of less than 11 dB at a wavelength of 1.55 μm, including an intrinsic polarization-division loss of 3 dB. Figure 13 shows

Table 2 Typical characteristics of the fabricated DP-QPSK modulator.

Parameters	Properties	Target spec.
Insertion loss	10.3 dB	< 14 dB
Extinction ratio; Parent MZI	32 dB	> 22 dB
Child MZI	27 dB	> 20 dB
Optical return loss	46 dB	> 30 dB
Polarization extinction ratio	38 dB	> 20 dB
PDL	0.4 dB	< 1.5 dB
EO bandwidth	27 GHz	> 23 GHz
RF port Vπ @ 32Gbaud	3.4 V	< 3.5 V

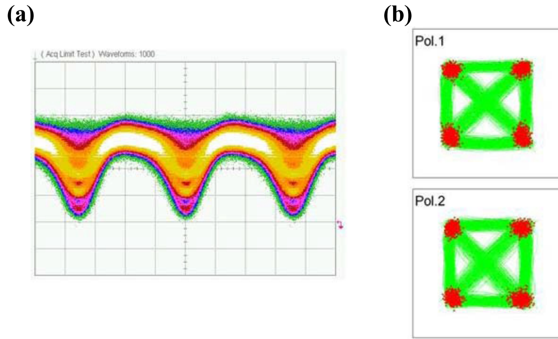

Fig. 13 (a) Measured eye diagram, (b) constellations of X-pol (Pol.1) and Y-pol (Pol.2).

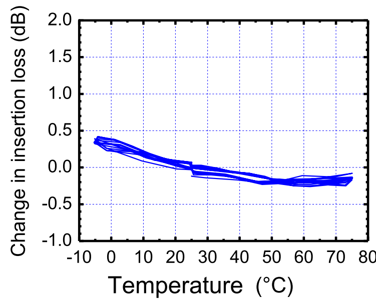

Fig. 14 Change in insertion loss during −5 to 75°C temperature cycle online test.

the good eye diagram and the clear constellations for the two channels, which correspond to two polarization channels.

4.2 Temperature Dependence

To confirm the validity of the selection of a waveguide pitch of 300 μm, as described in Sect. 3, we performed on-line temperature cycling tests between −5 and 75°C, which is the typical operation temperature range for a general 100-Gb/s optical transport system. Figure 14 shows the fiber-to-fiber insertion loss change in the temperature cycling test for ten cycles. The change was less than ±0.5 dB. The loss change is a little larger than our idealistic model in Fig. 6. We suppose that the excess loss is mainly added in the low temperature range originating from the misalignment of the waveguides in the PLC-LN assembly and the misalignment in out-of-plane movement in the temperature cycling process. Furthermore, we also measured the extinction ratio (ER) in the temperature change. Figures 15 and 16 show the extinction ratios of the Mach-Zehnder interference at 75, 25, and −5°C for X-polarization and Y-polarization, respectively. The amount of fluctuation is shown with reference to 25°C. These fluctuations are less than ±1 dB, and the stability in temperature change is obtained.

These results indicate that the insertion excess loss caused by the waveguide position shift with changing temperature is sufficiently suppressed in the operating temperature range.

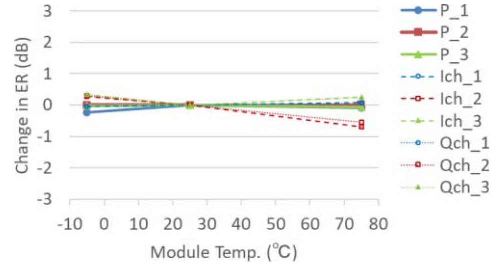

Fig. 15 Change in X-pol. extinction ratio of parent MZI and child MZI (Ich and Qch).

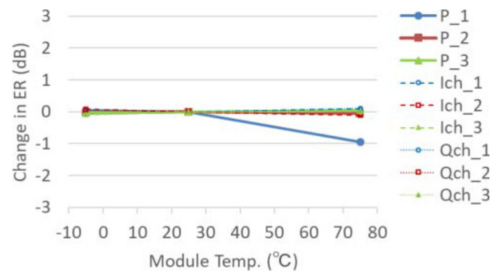

Fig. 16 Change in Y-pol. extinction ratio of parent MZI and MZI (Ich and Qch).

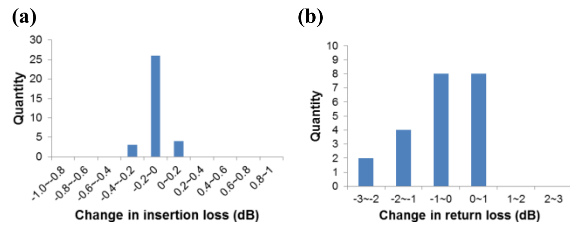

Fig. 17 Change in (a) insertion loss and (b) return loss after the mechanical shock test at 500 G.

4.3 Initial Strength Tests

We performed mechanical shock tests to confirm the reliability of hybrid assembly by using adhesive to silica-LN. We measured the characteristic for 11 modules before and after the test at 500 G. Figure 17 (a) shows the histogram of the changes in insertion loss (X-pol, Y-pol, total). They are less than ±0.4 dB. Figure 17 (b) shows the histogram of the changes in return loss for the input and output fiber. They are less than +1 dB and −3 dB, of course in specification. These results mean the initial strength of the hybrid modules is sufficient for the practical modules.

For our structure of a silica-LN hybrid modulator, the joint region between the PLC chip and LN chip might suffer from deterioration due to sympathetic vibration of the PLC chip, which is separated from the inside wall of the package. The natural vibration frequency of the PLC chip is determined by its size and the adhesive area between the PLC chip and LN chip. We optimized these parameters with which the PLC has a natural vibration frequency of over 2000 Hz using the finite element method. As in

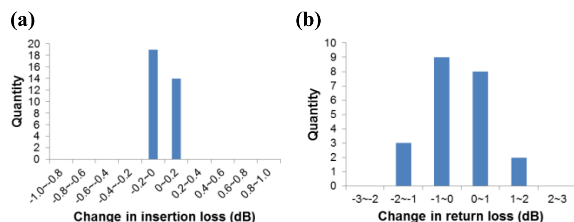

Fig. 18 Change in (a) insertion loss and (b) return loss after the vibration test between 20 and 2000 Hz at 20 G.

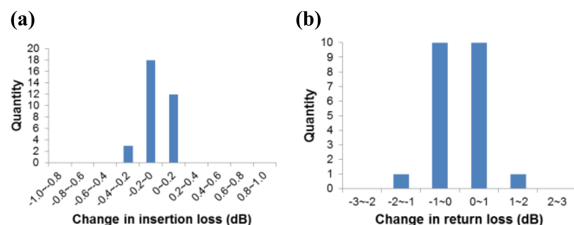

Fig. 19 Change in (a) insertion loss and (b) return loss after the temperature cycling tests between −40 and 85°C.

mechanical shock test, we measured the characteristic for 11 modules before and after the vibration test between 20 and 2000 Hz at 20 G. Figure 18 shows the histograms of the changes in insertion loss and in return loss. The former are less than ±0.2 dB, and the latter are less than ±2 dB. In addition, we performed an on-line test for the insertion loss and confirmed that the insertion loss variations are smaller than 0.1 dB. These results indicate that our hybrid modules are sufficiently resistant to vibration.

4.4 Temperature Cycle Tests

Furthermore, we also performed temperature cycling tests compliant with Telcordia-0468. Figure 19 is the histograms of the results of 100 temperature cycles between −40 and 85°C with a minimum temperature ramp rate of 10°C /min. The changes in insertion and return loss before and after cycling were at most ±0.4 and ±1.2 dB, respectively. We also checked that the extinction ratios after the test were within the specification. We confirmed the validity of our design guidelines to avoid the temperature change degradation associated with temperature change, which is the top issue for putting hybrid modules into practical use.

4.5 Other Environmental Tests

In addition to the above tests, we performed the other important Telcordia-0468 tests as shown in Table 3. After each test, we measured the optical insertion loss, optical return loss, polarization-dependent loss (PDL), on/off extinction ratio, polarization extinction ratio, DC $V\pi$, and photodiode responsivity. After all of tests, we measured the internal moisture. Table 4 shows the criteria for each module parameter after the tests. For these tests, we found that all of the silica-LN 100G DP-QPSK modules are reliable. These results specifically show that our silica-LN hybrid modulators, fabricated by following our proposed design guidelines, have sufficient reliability for practical use.

Table 3 Reliability test results compliant with Telcordia-0468.

Item	Test condition (GR-468)	Sample	Failure	Remark
Mechanical shock	300G, 3ms, 5times/direction	11	0	OK
Vibration	20G, 20-2000-20Hz 4min/cyc, 4cyc/axis	11	0	OK
Dump heat	85degC, 85%, 2000h	11	0	OK
Temp. Cycling	-40/85degC, 100cycle >= 10C/min	11	0	OK
High Temp. storege	85degC, 1500/2000h	11	0	OK
Cyclic Temp. Humidity	20 cyc, 25-65C, 80-100%RH,	11	0	OK
Thermal shock	Cond. A, 0-100C, 15cyc .	11	0	OK
Dump heat operational	75C, 85%, 1000h	11	0	OK

Table 4 Criteria for the environmental tests.

Item	Criteria
Insertion loss	Change < 1.0 dB
Reflection loss	In spec. after tests
PDL	Change < 0.5 dB
Extinction ratio	In spec. after tests
Polarization extinction ratio	In spec. after tests
DC Vpi	Change < 1.0 V
PD responsivity	Change < 15 mA/W
Internal Moisture	< 5000 ppm

5. Conclusion

For the fabrication of highly reliable silica-LN hybrid modulators, we proposed design guidelines for waveguide pitch, fiber thrust distance, and fiber feed length. We fabricated several tens of 100-Gbit/s DP-QPSK hybrid modulator modules based on the guidelines and confirmed their reliability in some important environmental tests based on Telcordia-0468. The guidelines are applicable to all other silica-LN hybrid modulators for more advanced formats.

Acknowledgments

The authors thank S. Sohma, T. Terui, S. Suzuki, and K. Shikama for their helpful advice and fruitful discussions on reliability tests of the modulators.

References

[1] T. Yamada, Y. Sakamaki, T. Shibata, A. Kaneko, A. Sano, and Y. Miyamoto, "Compact 111-Gb/s integrated RZ-DQPSK modulator using hybrid assembly technique with silica-based PLCs and

$LiNbO_3$ devices," Proc. OFC/NFOEC2008, San Diego, CA, USA, OThC3, 2008.
[2] H. Yamazaki, T. Yamada, K. Suzuki, T. Goh, A. Kaneko, A. Sano, E. Yamada, and Y. Miyamoto, "Integrated 100-Gb/s PDM-QPSK modulator using a hybrid assembly technique with silica-based PLCs and $LiNbO_3$ phase modulators," Proc. ECOC2008, Brussels, Belgium, Mo.3.C.1, 2008.
[3] H. Yamazaki, T. Goh, T. Saida, Y. Hashizume, S. Mino, M. Nagatani, H. Nosaka, and K. Murata, "Dual-carrier dual-polarization IQ modulator driven with high-speed DACs for 400-Gb/s applications," Proc. ECOC2012, Amsterdam, Netherlands, We.3.E.1, 2012.
[4] H. Yamazaki, T. Goh, A. Mori, and S. Mino, "Modulation-level-selectable optical modulator with a hybrid configuration of silica PLCs and $LiNbO_3$ phase modulators," Proc. ECOC2010, Torino, Italy, We.8.E.1, 2010.
[5] T. Goh, H. Yamazaki, T. Kominato, and S. Mino, "Novel flexible-format optical modulator with selectable combinations of carrier numbers and modulation levels based on silica-PLC and $LiNbO_3$ hybrid integration," Proc. OFC/NFOEC 2011, Los Angeles, CA, USA, OWV2, 2011.
[6] H. Yamazaki, T. Goh, T. Saida, Y. Hashizume, and S. Mino, "IQ-Coupling-Loss-Free Polarization-Switched QPSK Modulator," Proc. OFC/NFOEC 2012, Los Angeles, CA, USA, PDP5A.8, 2012.
[7] H. Yamazaki, T. Yamada, T. Goh, Y. Sakamaki, and A. Kaneko, "64QAM modulator with a hybrid configuration of silica PLCs and $LiNbO_3$ phase modulators," IEEE Photon. Technol. Lett., vol.22, no.5, pp.344–346, 2010.
[8] A. Sano et al., "240-Gb/s polarization-multiplexed 64-QAM modulation and blind detection using PLC-LN hybrid integrated modulator and digital coherent receiver," Proc. ECOC2009, Vienna, Austria, PD2.2, 2009.
[9] H. Yamazaki, H. Takahashi, T. Goh, Y. Hashizume, S. Mino, and Y. Miyamoto, "Linear Optical IQ Modulator for High-Order Multilevel Coherent Transmission," Proc. OFC/NFOEC 2013, Anaheim, CA, USA, OM3C.1, 2013.
[10] H. Yamazaki, Y. Hashizume, and T. Saida, "Simple Three--dimensional Simplex Modulator," Proc. OFC/NFOEC 2014, Anaheim, CA, USA, W1I.3, 2014.
[11] K. Tsuzuki, T. Saida, M. Ishii, T. Goh, H. Yamazaki, Y. Doi, A. Aratake, T. Fukumitsu, M. Tamura, and S. Mino, "Design and evaluation of highly reliable silica-$LiNbO_3$ hybrid modulators for advanced formats," Proc. OFC/NFOEC 2012, Los Angeles, CA, USA, OM3J.5, 2012.
[12] N. Kashima, "Reliability of optical cable with fusion splicing method," IEICE Technical Report, R95-44, 1996-02, 1996.
[13] F. Carter, Fluoride Glass Optical Fibres, ed. France, Ch. 9, pp.219–227, 1990.
[14] M. Kobayashi, "Research on optical assembly technologies for optical board," Dr. thesis, Nagoya University, p.92, 2002.
[15] Shin-Etsu Quartz Products Co., Ltd., "Technical guide of silica grass; Chemical and physical properties of silica grass [in Japanese]," [Online]. Available: https://www.sqp.co.jp/catalog/images/Technology_Guide1_j.pdf
[16] M. Kobayashi, "Research on optical assembly technologies for optical board," Dr. thesis, Nagoya University, p.88, 2002.

Atsushi Aratake was born in Miyazaki, Japan, in 1972. He received the B.E. and M.E. degrees in nuclear engineering from Kyoto University, Kyoto, Japan, in 1995 and 1997, respectively. In 1997, he joined the NTT System Electronics Laboratories, Atsugi, Japan, where he undertook research on advanced interconnection for ultrahigh-speed devices. From 2004 to 2007, he was involved in research on the reliability of PLC-type optical components at NTT Photonics Laboratories, Atsugi. In 2007, he moved to the Research and Development Planning Department, Tokyo, Japan, where he was involved in project and resource management for NTT R&D. From 2010 to 2011, he was with the NTT Photonics Laboratories, Atsugi, where he developed assembly technologies for silica-$LiNbO_3$ hybrid modulators and 100-Gb/s optical receiver front-end modules. He was a Senior Research Engineer, Supervisor at NTT Device Technology Laboratories, Atsugi in 2019. He is now with NTT Access Network Service Systems Laboratories, Tsukuba. Mr. Aratake is a senior member of the Institute of Electronics Information and Communication Engineers (IEICE) of Japan, and a member of the Japan Institute of Electronics Packaging.

Ken Tsuzuki received the B.S., M.S., and Ph.D. degrees in applied physics from Tohoku University in 1993, 1995, and 2006, respectively. In 1995, he joined NTT Opto-electronics Laboratories. Since then, he has been engaged in research and development on semiconductor photonic devices for optical fiber communications systems. From 2001 to 2002, he was with NTT Electronics Corporation. He is currently with NTT Device Innovation Center, where he is involved in research and development of photonic link devices for the next generation of optical communications systems. Dr. Tsuzuki is a member of the Optical Society of America, the Institute of Electronics, Information and Communication Engineers (IEICE) of Japan, and the Japan Society of Applied Physics.

Motohaya Ishii received the B.E. degree in electronics and the M.E. and D.E. degrees in information systems from Kyushu University, Fukuoka, Japan, in 1989, 1991, and 2008, respectively. He joined NTT Corporation, Kanagawa, Japan, in 1991, where he was engaged in research on silica-based planar lightwave circuits (PLCs). He is currently with the NTT Electronics Corporation, Ibaraki, Japan. Dr. Ishii is a member of the Institute of Electronics, Information and Communication Engineers (IEICE) of Japan.

Takashi Saida received the B.S., M.S., and Ph.D. degrees in electrical engineering from Tokyo University in 1993, 1995, and 1998, respectively. In 1998, he joined Nippon Telegraph and Telephone Corporation (NTT), where he was involved in research and development on functional silica-based planar lightwave circuits. From 2002 to 2003, he was a visiting scholar at Stanford University on leave from NTT laboratories. From 2006 to 2009, he was the Director at NTT Electronics Corporation. He is now with NTT Network Innovation Laboratories, where he is involved in research and development of next generation photonic transport technologies. Dr. Saida is a member of the IEICE, JSAP and IEEE, and a fellow member of OSA.

Takashi Goh received the B.S. and M.S. degrees in electronic and communication engineering from Waseda University, Tokyo, Japan, in 1991 and 1993, respectively. In 1993, he joined NTT Opto-electronics Laboratories, Ibaraki, Japan, where he was involved in research on silica-based planar lightwave circuits (PLCs). From 2002 to 2004, he was engaged in development of optical communication systems in NTT Innovation Laboratories, Yokosuka, Japan. From 2004 to 2017, he was with NTT Photonics Laboratories and Device Technology Laboratories, Atsugi, Japan, where he was involved in the research and development of integrated optical devices based on PLC technology for optical transmission and optical signal processing. He is currently with NTT Device Innovation Center, Kanagawa, Japan. He received the Young Engineer Award from the Institute of Electronics, Information and Communication Engineers (IEICE) of Japan in 2000. He is a member of IEICE, the IEEE Photonics Society, the Japan Society of Applied Physics, and the Physical Society of Japan.

Yoshiyuki Doi received the B.S. and M.S. degrees in physics, and Ph.D. degree in material science from Shinshu University, Nagano, Japan, in 1995, 1997 and 2007, respectively. He joined Nippon Telegraph and Telephone Corporation (NTT), Atsugi Opto-Electronics Laboratories in 1997. From 1997 to 2002, he was engaged in research on microwave photonics using a high-speed photonic millimeter-wave light source, phase-shift-keying modulator, and high-power emitting base station. Since 2002, He has been involved in the research and development of photonic devices and subsystems using hybrid integration on silica-based planar lightwave circuits (PLCs), such as high-speed receivers, large-scale optical switches, and high-functionality optical modulators. He is a Senior Research Engineer at NTT Device Innovation Center, Kanagawa, Japan. Dr. Doi is a member of the IEEE Photonics Society, IEEE Microwave Theory and Techniques Society as well as a member of Technical Coordinating Committees (TCC), and Information and Communication Engineers (IEICE) of Japan.

Hiroshi Yamazaki received the B.S. degree in integrated human studies in 2003 and the M.S. degree in human and environmental studies in 2005, both from Kyoto University, Kyoto, Japan, and Dr. Eng. degree in electronics and applied physics from Tokyo Institute of Technology, Tokyo, Japan, in 2015. In 2005, he joined NTT Photonics Laboratories, Kanagawa, Japan, where he has been involved in research on optical waveguide devices for communications systems. He is currently with NTT Device Technology Laboratories, Kanagawa, Japan, where he is involved in research on devices and systems for optical transmission using advanced multilevel modulation formats. Dr. Yamazaki is a member of the Institute of Electronics, Information and Communication Engineers (IEICE) of Japan.

Takao Fukumitsu received the B.S. degree in applied physics from University of Tsukuba, Tsukuba, Japan, in 1991. In 1991, he joined NTT Interdisciplinary Laboratories, Tokyo, Japan, where he was involved in research on devices for power electronics. In 1995, he moved to NTT Opto-electronics Laboratories, Ibaraki, Japan, where he was involved in research on assembly technologies and reliability of silica-based planar lightwave circuits containing reconfigurable add-drop multiplexers and silica-$LiNbO_3$ modulators. He is currently with NTT Device Technology Laboratories, Atsugi, Japan, where he has been involved in research on stress concentration and reliability of silica-based planar lightwave circuits. Mr. Fukumitsu is a member of the Institute of Electronics Information and Communication Engineers (IEICE) of Japan.

Takashi Yamada receivd B. E. and M. E. degrees from Tohoku University, Sendai, Japan, in 1994 and 1996, respectively. He joined NTT Opto-electronics Laboratories, Ibaraki, in 1996. From 2001 to 2009, he was engaged in research on high-speed optical functional modulators using hybrid assembly techniques with silica-based planar lightwave circuits and lithium niobate phase modulators. He is currently with NTT Device Innovation Center, Kanagawa, Japan, where he is involved in research and development of InP based DP-IQ modulators. Mr. Yamada is a member of the Institute of Electronics, Information and Communication Engineers (IEICE) of Japan.

Shinji Mino received the B.Sc. degree in chemistry from Waseda University in 1986, and an M.Sc., and Ph.D. in chemistry and electronic engineering from Tokyo University in 1988 and 1996, respectively. In 1988, he joined NT T Photonics Laboratories, Japan. He was engaged in the research and development of the hybrid-integration technology of silica-based PLCs and various active devices such as LDs and PDs, $LiNbO_3$ modulators, liquid crystal devices, and electronic ICs. Since 2009, he has been engaged in research and development of silica-$LiNbO_3$ hybrid-integrated modulators for 100 Gb/s and beyond. He is currently an Engineering Assistant Manager, Photonic Component Business Group, NTT Electronics Corporation, Ibaraki. Dr. Mino is a Senior Member of the Information and Communication Engineers (IEICE) of Japan and the IEEE Photonics Society.